Arabian Journal for Science and Engineering (2021) 46:1001–1018
https://doi.org/10.1007/s13369-020-04789-9

RESEARCH ARTICLE-ELECTRICAL ENGINEERING

Modified Synchronous Reference Frame Control of Solar Photovoltaic-Based Microgrid for Power Quality Improvement

Avdhesh Kumar[1] · **Rachana Garg**[1] · **Priya Mahajan**[1]

Received: 29 January 2020 / Accepted: 12 July 2020 / Published online: 1 August 2020

Abstract
In this paper, solar photovoltaic (SPV)-based microgrid has been connected to grid. Modified synchronous reference frame control of PV inverter has been proposed to estimate reference current for power quality improvement. Conventionally, DC link voltage of the PV inverter is regulated using proportional integral (PI) controller, which suffers from undershoot/overshoot and long settling time during load variation. Intelligent control technique can be the better solution with more accuracy and fast dynamic response. In the present work, interval type-2 (IT-2)-based fuzzy logic controller (FLC) has been proposed to control inverter's DC link voltage. Performance of the grid-connected SPV system is analyzed using proposed IT-2 FLC and compared with conventional PI as well as type-1 FLC. It compensates the harmonics of the nonlinear load and maintains the grid at unity power factor by supplying the reactive demand of the load. Total harmonic distortion at grid side of the system is within the limits as per IEEE-519 standard. To test the efficacy of the proposed IT-2 FLC for grid-connected SPV system MATLAB software2016(a) has been used.

Keywords Power quality (PQ) · Interval type-2 (IT-2) · Fuzzy logic controller (FLC) · Photovoltaic (PV) array · Synchronous reference frame (SRF)

Abbreviations

DG	Distributed generation
RES	Renewable energy sources
SPV	Solar photovoltaic array
SRF	Synchronous reference frame
PQ	Power quality
THD	Total harmonic distortion
LPF	Low-pass filter
UPF	Unity power factor
PLL	Phase-locked loop
FLC	Fuzzy logic controller
IT-2	Interval type-2
V^*_{dc}	Reference DC link voltage
V_{dc}	Actual sensed DC link voltage
V_{sa},V_{sb}, V_{sc}	PCC or grid voltage of phases a, b and c
I_{la}, I_{lb}, I_{lc}	Load current of phases a, b and c
i_d	Active component of load current
i_{dloss}	Output of FLC
I^*_{sabc}	Reference current
PCC	Point of common coupling
HCC	Hysteresis current control

✉ Avdhesh Kumar
iesavd@gmail.com

Rachana Garg
rachana16100@yahoo.co.in

Priya Mahajan
priyamahajan.eed@gmail.com

[1] Electrical Engineering Department, Delhi Technological University, Bawana Road, Rohini, Delhi 110042, India

1 Introduction

Nowadays, the sources of sustainable and green energy such as renewable energy sources (RES) are ecological friendly and can be harnessed for distributed generation (DG). Among different RES, solar photovoltaic (SPV)-based power generation resolves the ecological issues like the global warming, greenhouse effect, etc. The SPV generation is becoming eminent due to ease of installation, low maintenance cost, learning skill, an adequate amount of resources, emerging technologies, etc. [1–6]. SPV system has been installed worldwide at a massive scale for power generation. Power generated using SPV system can be utilized locally and can be integrated with grid also. SPV integration to the utility grid faces challenges related to power quality like distortion in voltage/current, voltage fluctuations

and harmonics [7–9]. Due to grid integration of SPV system, harmonics are generated on both sides, viz., SPV (source) and common coupling point (PCC) of the system. However, harmonics injection from SPV system to grid is mainly due to switching of power electronics-based converter, degrading power quality of supply system [7, 10–12].

On the other hand, problem of PQ at PCC is introduced in the system due to the presence of various nonlinear loads and power electronic devices connected to PCC, which draw nonlinear current from system [7]. PQ is an important issue in both domestic applications and commercial/industrial applications. Power supplied by the SPV system is said to be of good quality when quality of power available at consumer end is within the limits of IEEE standards [13]. Total harmonic distortion (THD) level in grid current must be less than 5% according to practices recommended in IEEE-519 [12]. Moreover, voltage fluctuations as recommended by IEEE-1547 should be within ± 5% at PCC [14]. Therefore, it is very essential to develop an efficient control of grid-integrated SPV system with enhanced performance to keep PQ within acceptable limits of IEEE standards. Along with the grid integration of SPV system, it is also very challenging to get maximum power from SPV array under varying operating conditions. Thus, for SPV system an efficient maximum power point tracking (MPPT) control technique is needed. In the literature [4, 15–20], various conventional control algorithms of MPPT such as incremental conductance (INC), adaptive step size MPPT with single sensor and perturb & observe (P&O) are presented.

There are many conventional, intelligent and adaptive control techniques for reference current generation of grid integration with RES were reported in the literature [11, 21–24]. Many conventional control schemes, viz., SRF, instantaneous reactive power theory (IRPT) and power balance theory (PBT), have been implemented. A phase locked loop (PLL) is required to transform three phase *a*-*b*-*c* quantities to *d*-*q*-0 axis in SRF-based control, and it has to be tuned prior to its operation. Conventional SRF is one of the most practically applicable methods. Although due to conventional PLL, it exhibits poor performance under distorted and unbalance grid [25, 26]. In the literature [21, 26], it has been observed that performance of PLL is easily affected by distortions and noise and SOGI PLL has been proposed to overcome these drawbacks. In the implementation of IRPT, reference current is estimated using voltage and current of the PCC, so fluctuation in voltage will reflect in the reference current. Although control technique of reference current estimations of each algorithm is slightly different, but the control of DC link voltage in each conventional algorithm is by PI controller. Conventional control algorithms based on PI controller are not suitable for load variations as they suffer from undershoot/overshoot and long settling time. To overcome such problems, adaptive or intelligent control technique can be the better solution with more accuracy and fast dynamic response [27, 29]. Intelligent FLC control algorithm gives faster response to variation in input and load conditions [27–29]. Performance of a controller can be assessing harmonics in grid current, ripple free generation of reference and transient response of inverter's DC link voltage. As compared to a PI controller, type-1 FLC has better initial transient response, viz., undershoot/overshoot during the grid integration and load perturbation [27, 29]. Barik et al. [25] evaluated the power quality of distribution static compensator system using type-1 FLC. DC link voltage regulation and reduction in its settling time are realized by either PI or FLC or fuzzy-PI controller schemes in SRF-based designed control for shunt active filter. The settling time with proposed control scheme was 0.04 s, while with PI it was 0.10 s. The technique can be implemented to PV system tied to grid for enhanced power quality. Karuppanan et al. [26] proposed FLC-based control algorithm for estimating reference current using shunt active power filter for PQ improvement. THD and DC link settling time are small using FLC. In [30], authors have proposed Takagi–Sugeno Fuzzy to maintain voltage across DC link for enhance performance of standalone PV system connected to single-phase grid. The controller has been tested using MATLAB software. Authors in [31] presented adaptive fast sliding mode control for single-phase PV connected to grid using fuzzy neural network (FNN). The FNN updates its weight in accordance with uncertainties with system and minimizes the error. It is implemented on single-phase grid and has not been considered varying solar insolation, dynamic and unbalance load. In [32], predictive neural network controller (PNNC) with the aim to improve the PQ issues like harmonics within IEEE norms and DC link voltage regulation along with reactive power compensation is presented. The PNNC technique has been compared with PI controller, and it is found to be better than that of PI, while in the present work proposed IT-2FLC has been compared with PI and type-1 FLC. In [33], PI genetic algorithm-based control of grid integrated to PV system has been proposed to reduce the harmonics with UPF operation of the system. The genetic algorithm has been compared with PI controller and genetic algorithm found to be better than PI controller. Gupta et al. [27, 29] presented asymmetrical fuzzy logic control (FLC) for reference generation, shows that type-1 FLC is superior than conventional PI controller for the control of DC link voltage. However, type-1 FLC may not handle dynamic environment having linguistic and numerical uncertainties. FLCs exhibit obvious limitations such as their requirement on the user's knowledge about the system and complicated rules. The higher number of rules will increase the difficulty of FLC design and implementation [34]. Type-1 FLC is very challenging when these uncertainties are related to input, output which leads to uncertainties in the optimization of

fuzzy set membership functions. The limitations of type-1 FLC can be overcome by interval type (IT-2) FLCs which have the potential to optimize the fuzzy set membership function and give more efficient performance for grid integration of RES-based microgrid applications [35].

In the present manuscript work, the type-2 FLC has been implemented for SPV system connected to three-phase distribution grid under various input and loading conditions. Further, to establish the efficacy of the proposed control, it has been compared with conventional PI controller and type-1 FLC.

The major contributions of the present work as given below:

1. Design of novel type-2 FLC for SPV-based microgrid using modified SRF control is carried out for grid integration.
2. Proposed algorithm extracts, fundamental active component from load current to estimate reference current for grid integration. Transient response in DC link voltage of the system get improved.
3. Unity power factor operation at grid side by compensating the reactive power of the load.
4. Improving PQ by removing harmonics in the grid current thus helps in maintaining grid current sinusoidal and balance during the unbalanced loading condition by supplying current as per each phase requirement.
5. Performance of the proposed system is tested for linear/nonlinear (balance/unbalance) load under steady state and dynamic state and is compared with PI as well as type-1 FLC.

In this paper, SPV system is integrated with grid using inverter and its passive components. For the first time in the literature, Interval Type-2 FLC-based modified SRF control has been used for DC link voltage regulation. IT-2 FLC control is robust to uncertainties of input parameter variations in PV array and gives better transient response of DC link voltage along with improved PQ of the system. The proposed controller is modeled and simulated in MATLAB software2016(a). Evaluation of proposed IT-2 FLC controller is carried out and is compared with conventional PI controller and type-1 FLC. Performance of proposed IT-2 FLC control is analyzed under varying atmospheric condition. IT-2 FLC can manage those uncertainties in order to provide more efficient performance. The results were evaluated in accordance with IEEE-1547 and IEEE-519.

Topology of the SPV-based grid-integrated microgrid presented in Fig. 1 demonstrates proposed 10.25 kW SPV-based microgrid system configuration. System consists of SPV array, DC–DC boost converter, MPPT, three-phase inverter with its passive components and various loads connected at point of common coupling (PCC). Source voltage of boost converter is not constant due to variable input of PV array such as solar insolation and temperature. Therefore, to get the constant output voltage and maximum power, MPPT defines suitable duty cycle which regulates output voltage of boost converter corresponding to maximum power of PV array, and thus, PV array output power is regulated. Voltage across DC link is controlled by IT-2 FLC. Grid integration of solar PV array is accomplished using modified SRF inverter control.

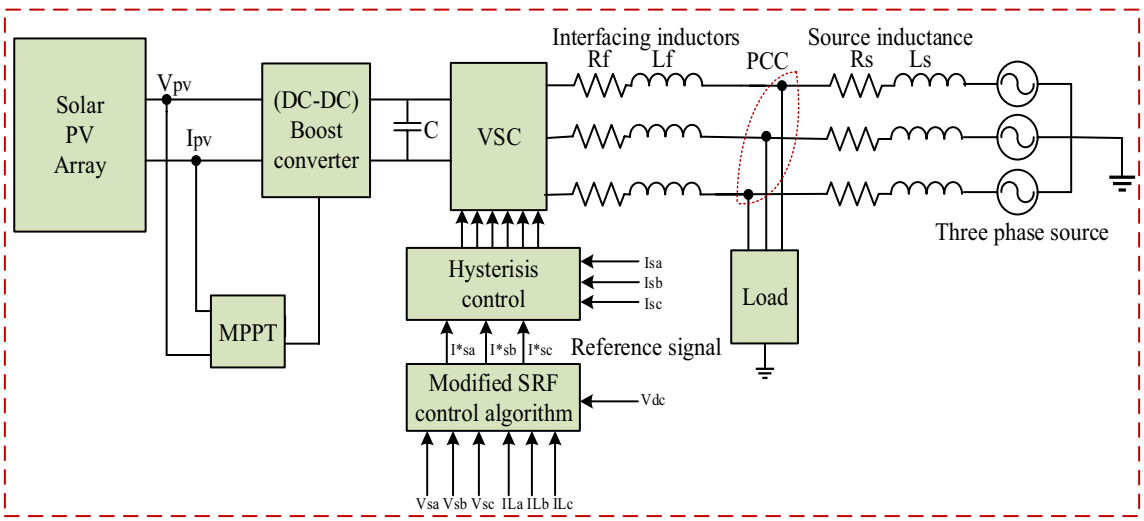

Fig. 1 Proposed solar PV-based microgrid system configuration

2 Inverter Control Technique

2.1 SRF Theory of Inverter Control

Reference current for inverter is generated using SRF theory of inverter control technique. In this technique, active (i_d) and reactive (i_q) load current components are extracted, respectively. SRF theory uses load current in the *a-b-c* frame to *d-q*-0 to extract active and reactive components of load current. Three-phase current in the a-b-c frame is transformed into *d-q*-0 frame by means of Park's conversion:

$$\begin{bmatrix} i_d \\ i_q \\ i_0 \end{bmatrix} = (2/3)\begin{bmatrix} \cos\ \mathrm{wt} & \cos(\mathrm{wt}-120) & \cos(\mathrm{wt}+120) \\ \sin\ \mathrm{wt} & \sin(\mathrm{wt}-120) & \sin(\mathrm{wt}+120) \\ 1/2 & 1/2 & 1/2 \end{bmatrix}\begin{bmatrix} i_{la} \\ i_{lb} \\ i_{lc} \end{bmatrix} \tag{1}$$

where wt and i are the transformation angle and current, respectively. Low-pass filter is connected to extract DC quantities of active (i_d) and reactive (i_q) component of load. To synchrnous microgrid signal with the grid, three phase locked loop (PLL) is required. This algorithm uses PI controllers to keep the constant voltage across dc link. However, in the present work modified SRF IT-2 FLC is used. Figure 2 demonstrates the modified SRF-based inverter control to produce reference current. Inverter is operated in unity power factor mode (UPF) mode in the present work.

2.1.1 UPF Operation of Grid-Connected Solar PV-Based Microgrid

In UPF mode of operation, improvement in power factor is achieved by compensating reactive power. DC component of direct axis load current (i_d) with active power component must be supplied with this control approach in order to keep voltage across DC link as constant. Output of the PI controller (i_{dloss}) is added with DC quantities of active component (i_d) from load current.

$$i_{\mathrm{d}}^{*} = i_{\mathrm{id}} + i_{\mathrm{dloss}} \tag{2}$$

Generated reference current (i^{*}_{sabc}) must be in same phase with grid voltage, using reverse Park's conversion as represented below, i^{*}_{sabc} are obtained:

$$\begin{bmatrix} i_{sa}^{*} \\ i_{sb}^{*} \\ i_{sc}^{*} \end{bmatrix} = \begin{bmatrix} \cos\ \mathrm{wt} & \sin\ \mathrm{wt} & 1 \\ \cos(\mathrm{wt}-120) & \sin(\mathrm{wt}-120) & 1 \\ \cos(\mathrm{wt}+120) & \sin(\mathrm{wt}+120) & 1 \end{bmatrix}\begin{bmatrix} i_d \\ i_q \\ i_0 \end{bmatrix} \tag{3}$$

Figure 2 depicts the modified SRF control of PV inverter. Here, the conventional PI control is replaced by IT-2 FLC.

2.2 Design of Type-1 FLC

In conventional SRF inverter control technique, DC link control is achieved using conventional PI controller. In a system with nonlinear loads, conventional PI controller does not exhibit efficient performance toward settling time and overshoot/undershoot. Further, FLC gives better performance under nonlinearities [20]. Basic concept in FLC, which plays an important role in most of its applications, is that of a fuzzy IF–THEN rule. Membership functions are assigned to input and output variables. Input membership function of FLC and its proper designed rule base gives improved dynamic performance of the system [22]. Mamdani FLC has been used for inferencing the input of the designed type-1 FLC (Fig. 3). In design of type-1 FLC controller for inverter, five sets of triangular membership functions are used, as negative big: –B, negative medium: –M, zero: Z, positive medium: +M, positive big: +B. rule base is shown in Table 1.

2.3 Design of Proposed IT-2 FLC

In the present studies, IT-2 FLC has been proposed to regulate the DC link voltage of grid-integrated SPV system. Proposed IT-2 FLC-based control block diagram of DC link

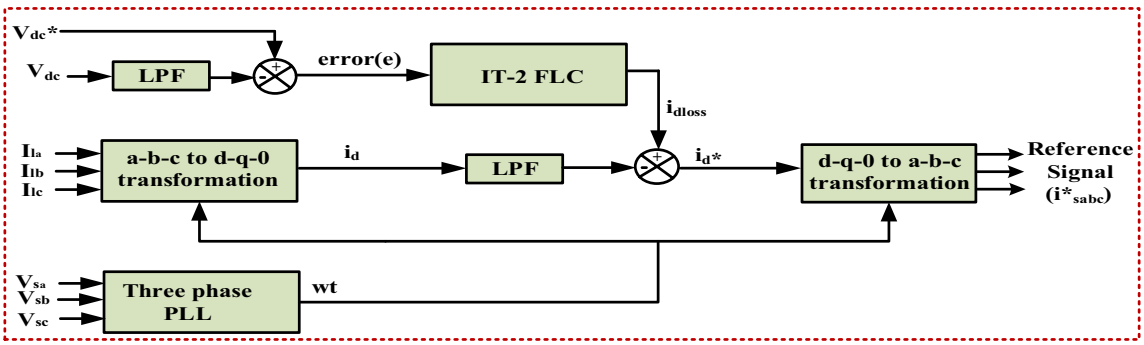

Fig. 2 Proposed modified SRF control algorithm for reference generation of PV inverter

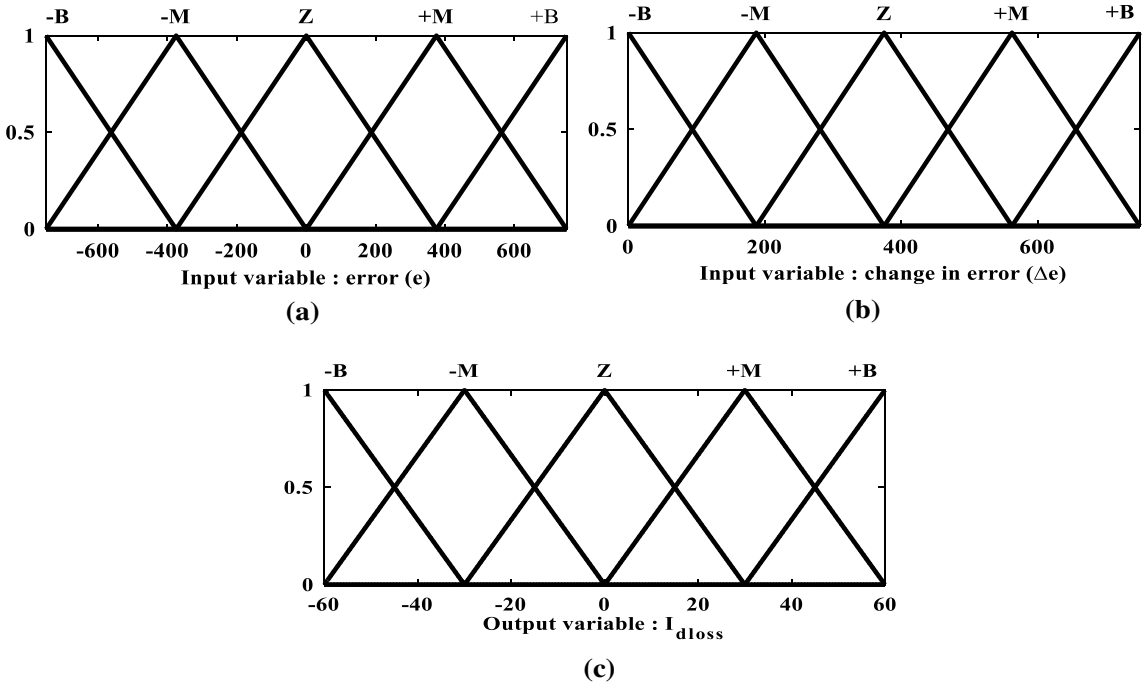

Fig. 3 Membership function of type-1 FLC for computing i_{dloss}, input variable: **a** error, **b** change in error, **c** output variable: i_{dloss}

Table 1 Fuzzy rule base for computing i_{dloss}

Error(e) \ change in error (Δe)	$-B$	$-M$	Z	$+M$	$+B$
$-B$	$-B$	$-M$	$-M$	Z	$+M$
$-M$	$-M$	$-M$	Z	$+M$	$+B$
Z	$-M$	Z	$+M$	$+B$	$+B$
$+M$	Z	$+M$	$+B$	$+B$	$+B$
$+B$	$+M$	$+B$	$+B$	$+B$	$+B$

voltage of inverter is shown in Fig. 4a. Controller has two input variables:$e(k)$, $\Delta e(k)$ and one output variable (i_{dloss}).

$$e(k) = V_{\text{dc}}^{*} - V_{\text{dc}}(k) \tag{4}$$

$$\Delta e(k) = e(k) - e(k-1) \tag{5}$$

where V_{dc}^{*} is reference DC link voltage and $V_{\text{dc}}(k)$ is actual sensed DC link voltage at k_{th} iteration, $e(k)$ and $\Delta e(k)$ are error and change in error, respectively, at k_{th} iteration [27, 29].

Structure of proposed controller along with, description of each block, viz., fuzzification, rule base and defuzzification involving type reduction is presented. Error ($e(k)$) and change in error ($\Delta e(k)$) represent input variables and i_{dloss} as an output variable.

IT-2 FLC has four stages: fuzzification, rule base, inferencing and output processing which are explained below:

2.3.1 Interval Type-2 fuzzification

Figure 5 represents an example for fuzzification of IT-2 FLC. IT-2 FLC membership value in the [0, 1] domain is defined for each input. For each input, two membership levels are computed, and one is called the upper membership function (UMF) and other lower membership function (LMF). Interval type-2 FLC with an extra dimension called footprint of uncertainty (FOU) is capable of handling large amount of uncertainty. In Fig. 5 when $e\,(k)=\alpha_1^{'}$, a vertical line at $\alpha_1^{'}$ intersects FOU ($\tilde{P}$) everywhere in the interval $[\underline{S}_{\tilde{P}}(\alpha_1^{'}), \bar{S}_{\tilde{P}}(\alpha_1^{'})]$ and when $\Delta e(k)=\alpha_2^{'}$, vertical line at $\alpha_2^{'}$ intersects, FOU ($\tilde{Q}$) everywhere in the interval $[\underline{S}_{\tilde{Q}}(\alpha_2^{'}), \bar{S}_{\tilde{Q}}(\alpha_2^{'})]$.

2.3.2 Rule Base and Inference System

In the design of rule base of IT-2 FLC for inverter, five sets of triangular membership function are used, as negative big: ((–*B* (*U*/*L*)), negative medium (–*M* (*U*/*L*)), zero (Z (U/L)), positive medium (+*M* (*U*/*L*))), positive big (+*B* (*U*/*L*)). Interval type-2 fuzzy rule base for proposed controller is written in the equation given below:

$$\text{IF } e(k) \text{ is } \tilde{P} \text{ and } \Delta e(k) \text{ is } \tilde{Q} \text{ THEN output is } \tilde{R} \tag{6}$$

where $\tilde{P}$ and $\tilde{Q}$ are IT-2 fuzzy sets and $\tilde{R}$ is output. Therefore, using Eq. (6), 25 rule bases have been developed for computation of i_{dloss} as shown in Table 2.

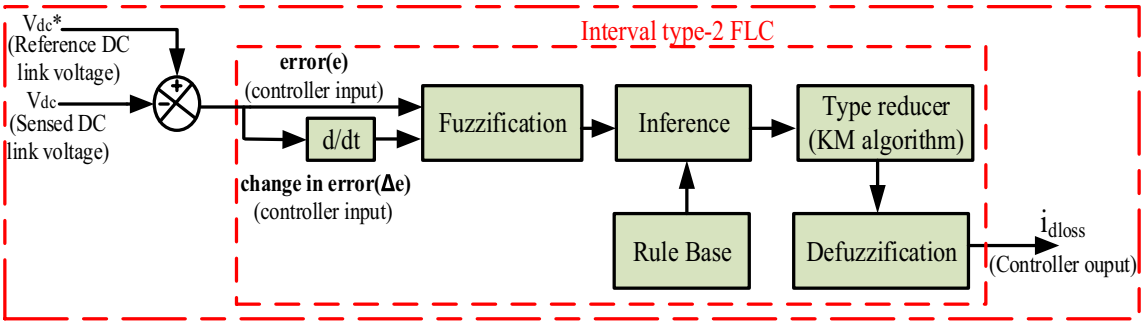

(a) Proposed interval type-2 FLC for DC link voltage control of inverter

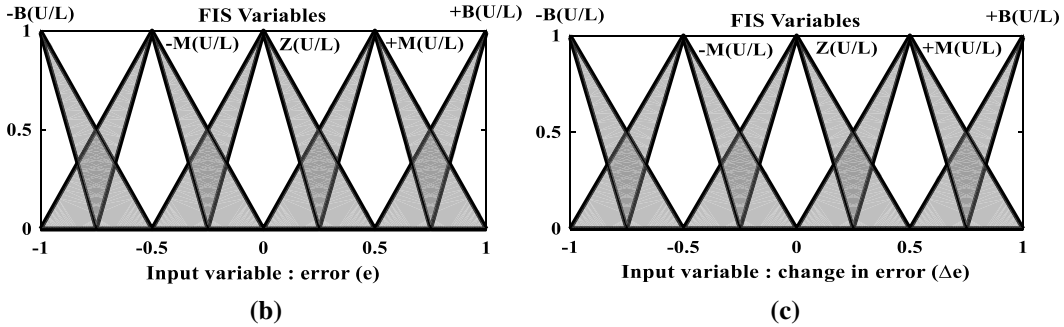

(b) **(c)**

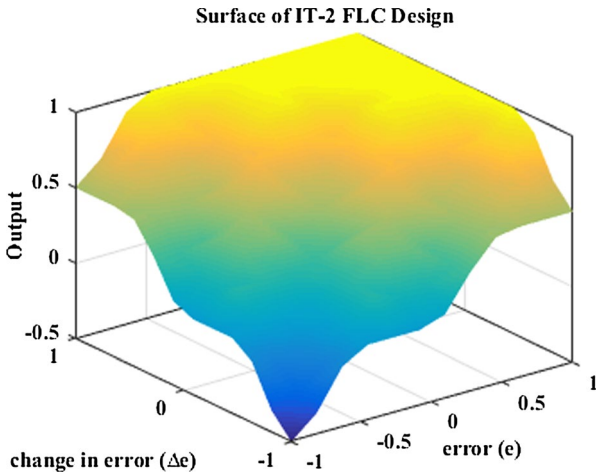

(d)

Fig. 4 **a** block diagram of proposed interval type-2 FLC, **b** and **c** membership function for input variable 'error' and 'change in error,' respectively, and **d** surface view of IT-2 fuzzy logic design

Inference process combines rule and gives mapping from input to output. For a single rule, inference process is shown in Fig. 5. Two firing levels are then computed, an upper firing level, $\bar{f}$ and a lower firing level $\underline{f}$, where $\bar{f} = \min[\bar{S}_P^{\sim}(\alpha_1'), \bar{S}_Q^{\sim}(\alpha_2')]$ and $\underline{f} = \min[\underline{S}_P^{\sim}(\alpha_1'), \underline{S}_Q^{\sim}(\alpha_2')]$.

2.3.3 Type Reduction and Defuzzification

Type 1 fuzzy set is generated by type reduction, and the reduced fuzzy set is converted into crisp value in defuzzification stage. In the present work, Karnik–Mendel (KM) algorithm has been used for type reduction and defuzzification.

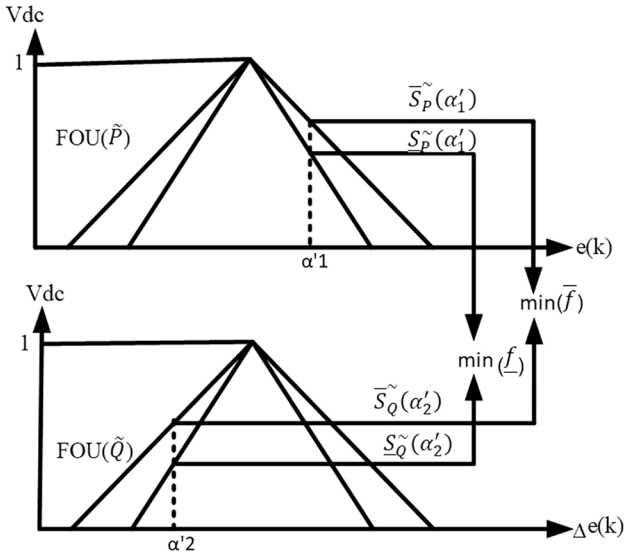

Fig. 5 Fuzzification and inference of IT-2 FLC

Table 2 Rule base for IT-2 FLC

Error(e)\ change in error (Δe)	–B (U/L)	–M (U/L))	Z (U/L)	+M (U/L))	+B (U/L)
–B (U/L)	–M (U/L))	Z(U/L)	Z(U/L)	+M(U/L)	+M(U/L)
–M (U/L))	Z(U/L)	Z(U/L)	+M(U/L)	+M(U/L)	+B(U/L)
Z (U/L)	Z(U/L)	+M(U/L)	+M(U/L)	+B(U/L)	+B(U/L)
+M (U/L))	+M(U/L)	+M(U/L)	+B(U/L)	+B(U/L)	+B(U/L)
+B (U/L)	+M(U/L)	+B(U/L)	+B(U/L)	+B(U/L)	+B(U/L)

3 Experimental Results

This section presents the simulation results and the corresponding discussion to grid-integrated SPV system. Performance of proposed controller IT-2 FLC is analyzed and compared with both type-1 FLC and conventional PI controller, respectively, under various atmospheric and load conditions. Current and voltage harmonics at PCC are minimized using proposed control technique. Proposed control is modeled in MATLAB/Simulink environment. The parameters of the system are given in Appendix A.

3.1 Performance of Solar PV-Based Grid-integrated System Using Proposed IT-2 FLC

3.1.1 Steady-State Behavior Under Linear and Nonlinear Load Condition at STC

The performance of grid-integrated SPV system at standard test condition (STC) using proposed IT-2 FLC under linear and nonlinear load condition is studied. Various parameters of the system, viz., grid voltage (V_{grid}), grid current (I_{grid}), load current (I_{load}), inverter current (I_{inv}), DC link voltage (V_{dc}) and real power sharing between grid, inverter and load are also analyzed and shown in Figs. 6 and 7, respectively.

A linear load of 5 kVA (4 kW and 3 kVAR) 0.8 pf lagging is connected to the system. It is observed from Fig. 6 that V_{grid} and I_{grid} are 180° out of phase (as power is fed to the grid), and V_{dc} is maintained at 750 V, SPV supplies 4 kW active power and 3 kVAR of reactive demand of the load. Load active and reactive power demand is supplied by inverter alone which reduces reactive power drawn from the grid to zero showing IT-2 FLC is efficient in maintaining grid at UPF. Further, remaining 6.25 kW power of the SPV system is fed back to the grid showing that as per the load requirement, active and reactive power is shared between load (P_{load}, Q_{load}), grid (P_{grid}, Q_{grid}) and inverter (P_{inv}, Q_{inv}).

Further, to test the robustness of the proposed control of SPV-based microgrid for a nonlinear load, a three-phase rectifier with RL load ($R = 100\ \Omega$, $L = 100$ mH) has been connected to the system and the results are shown in Fig. 7. From Fig. 7, it is observed that SPV system supplies its rated active power of 10.25 kW. Load active and reactive power demand is supplied by inverter alone which reduces reactive power drawn from the grid to zero, and hence, IT-2 FLC is efficient in maintaining grid at UPF. Further, remaining power of the SPV system is fed back to the grid. It is observed that as per the load requirement, active and reactive power is shared between load (P_{load}, Q_{load}), grid (P_{grid}, Q_{grid}) and inverter (P_{inv}, Q_{inv}). It is also observed that by using IT-2 FLC-based control of SPV-based microgrid, voltage and current harmonics are compensated in the utility grid system. The nonlinear load current and the corresponding THD profile are shown in Fig. 8c without compensation, which is observed to be very high equal to 28.28%. Further, from Fig. 8a, b, it is observed that THD in grid current is 1.64%, and 1.44%, respectively, under linear and nonlinear load condition, which is well within IEEE standard 519-2014.

3.1.2 Steady-State Behavior Under Linear and Nonlinear Load Condition at Varying Insolation

Further to test robustness of proposed IT-2 FLC, the controller is tested under linear/nonlinear load at varying insolation. Solar insolation is reduced at 0.15 s from 1000 to 700 W/m^2 till 0.25 s and again increased from 0.35 to 0.45 s till 1000 W/m^2). Due to decrease in solar insolation, solar PV current decreases that leads to decrease in output power of solar PV and vice versa. A linear load (20 kVA, 0.8 pf lag) is considered, and Fig. 9 shows the various system parameters, viz., V_{grid}, I_{grid}, I_{load}, I_{inv}, P_{grid}, Q_{grid}, P_{inv}, Q_{inv}, P_{load}, Q_{load} and V_{dc} for the considered load.

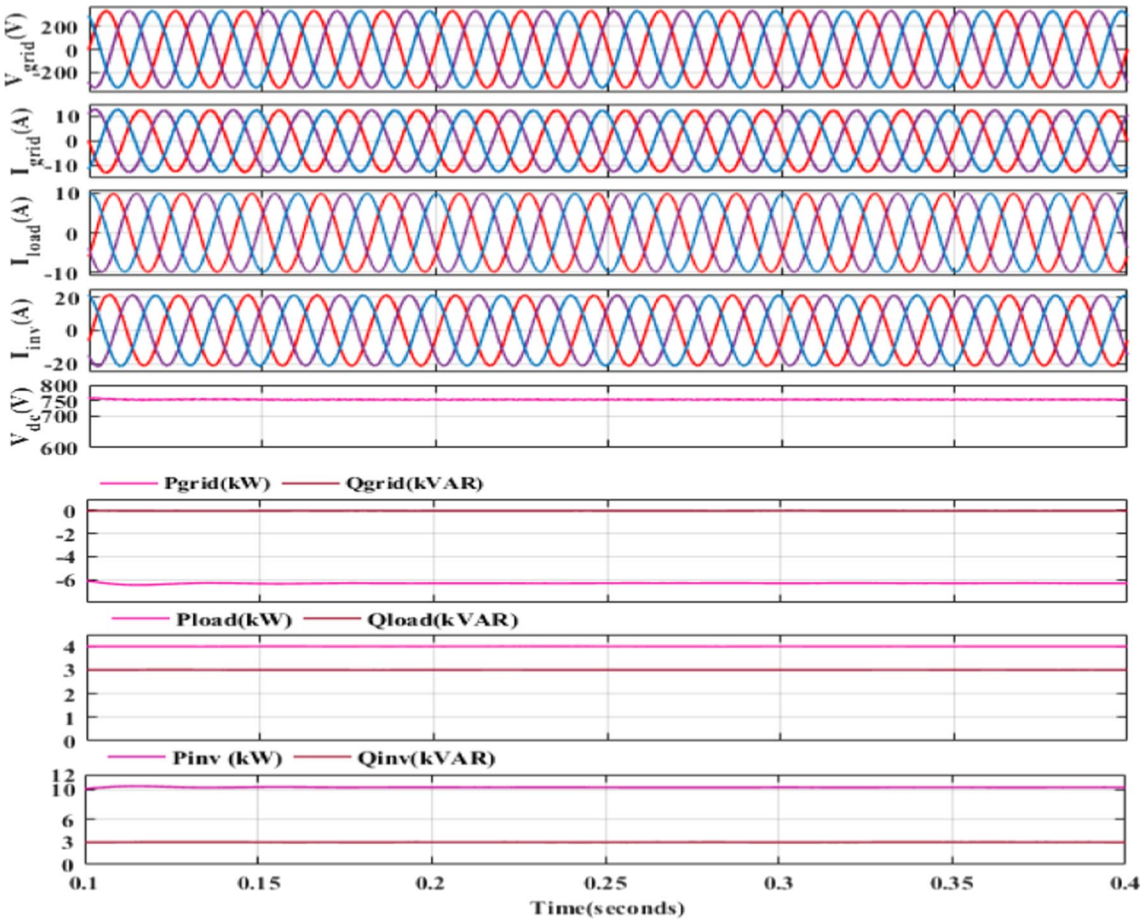

Fig. 6 Simulated performance of SPV-based microgrid under linear load at STC input

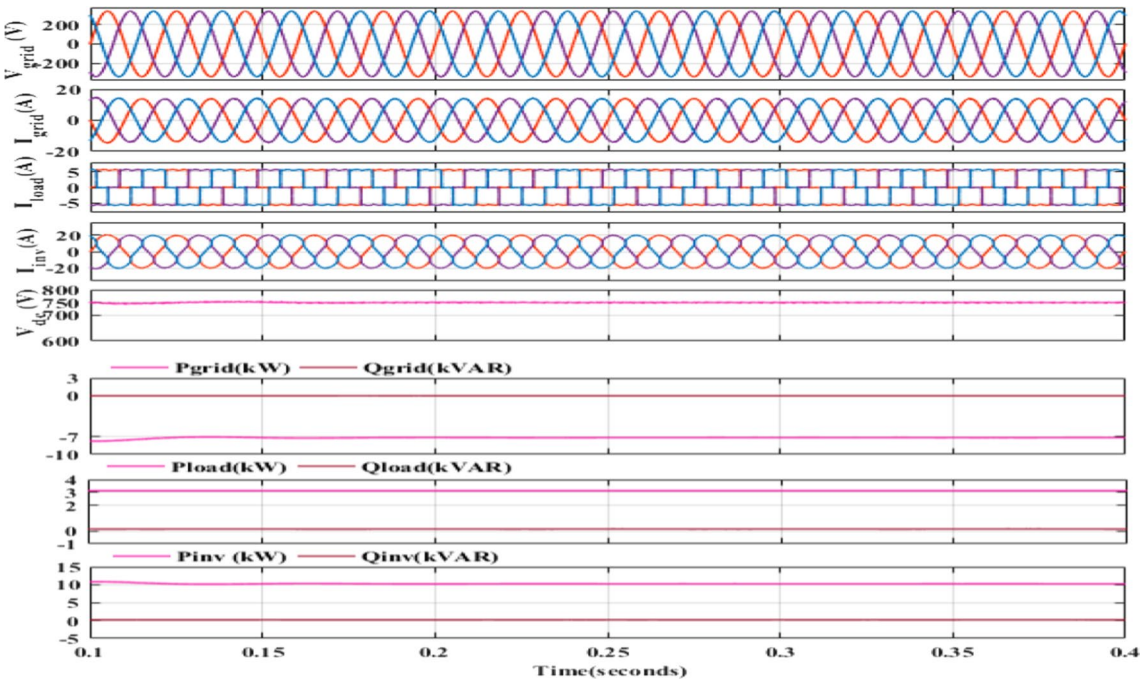

Fig. 7 Simulated performance of SPV-based microgrid under nonlinear load at STC input

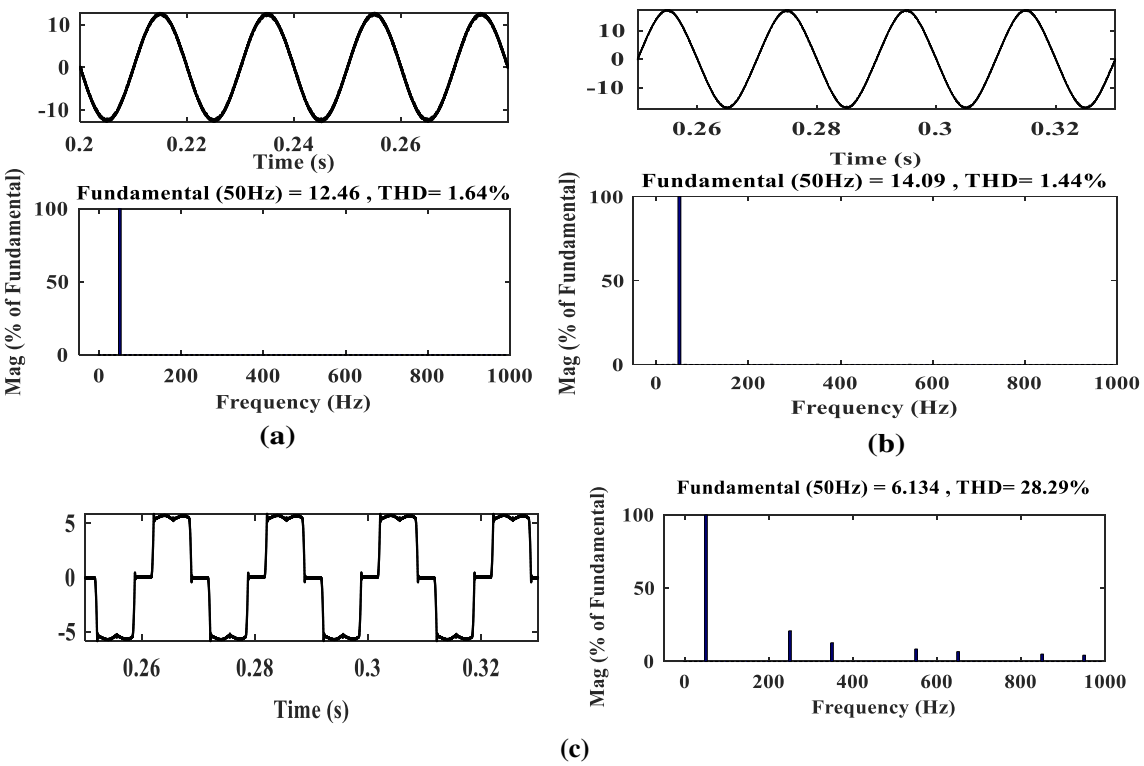

Fig. 8 Grid current waveform and THD at STC input: **a** with compensation under linear load, **b** with compensation under nonlinear load, **c** without compensation under nonlinear load

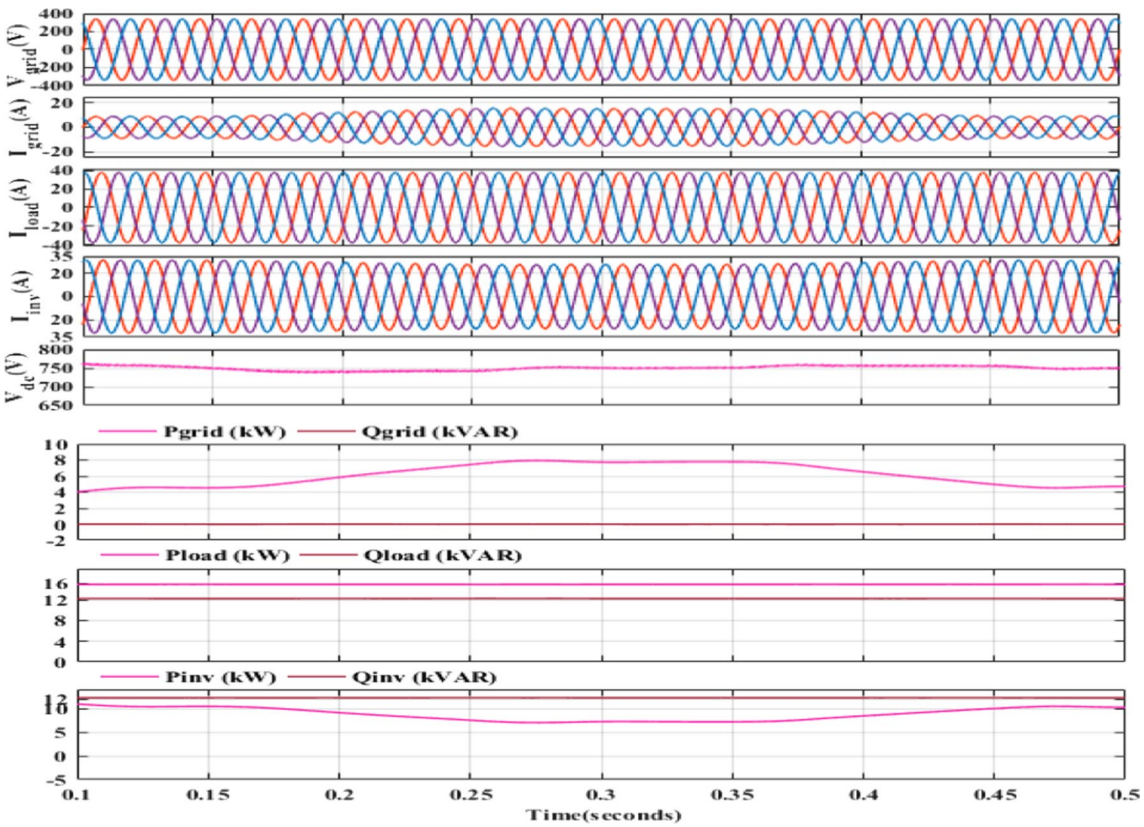

Fig. 9 Simulated performance of SPV-based microgrid under linear load at varying insolation

From Fig. 9, it is observed that both V_{grid} and I_{grid} are in phase, showing UPF operation using the proposed control. V_{dc} is maintained at 750 V. SPV supplies 10.25 kW of active load demand of 16 kW, while the remaining load demand of 5.75 kW is supplied by the grid, whereas total reactive power is supplied by inverter alone as shown in Fig. 9. From Fig. 11a and Table 3, it has been observed that THD in grid current and voltage for linear load, respectively, is within IEEE standard and system remains in stable condition, maintaining power sharing between inverter, grid and load.

Table 3 THD (%) in grid current and grid voltage at varying insolation

Scenario	Load current THD (%)	Grid current THD (%)	Grid voltage THD (%)
Linear load	–	2.87	1.09
Nonlinear load	28.76	2.45	0.92

For a nonlinear load, a three-phase bridge rectifier with RL (($R = 100\ \Omega$, $L = 100$ mH)) load is considered and and Fig. 10 shows various system parameters, viz., V_{grid}, I_{grid}, I_{load}, I_{inv}, P_{grid}, Q_{grid}, P_{inv}, Q_{inv}, P_{load}, Q_{load}, and V_{dc} for the considered load. It is observed from Fig. 10 grid is at UPF using proposed control. V_{dc} is maintained at 750 V. The reactive power demand of the load is supplied by inverter alone. Also, it is observed from Fig. 11b and Table 3 that using proposed control during the varying insolation, THD in V_{grid} and I_{grid} is 2.87 and 1.45, respectively, which is well within IEEE limits.

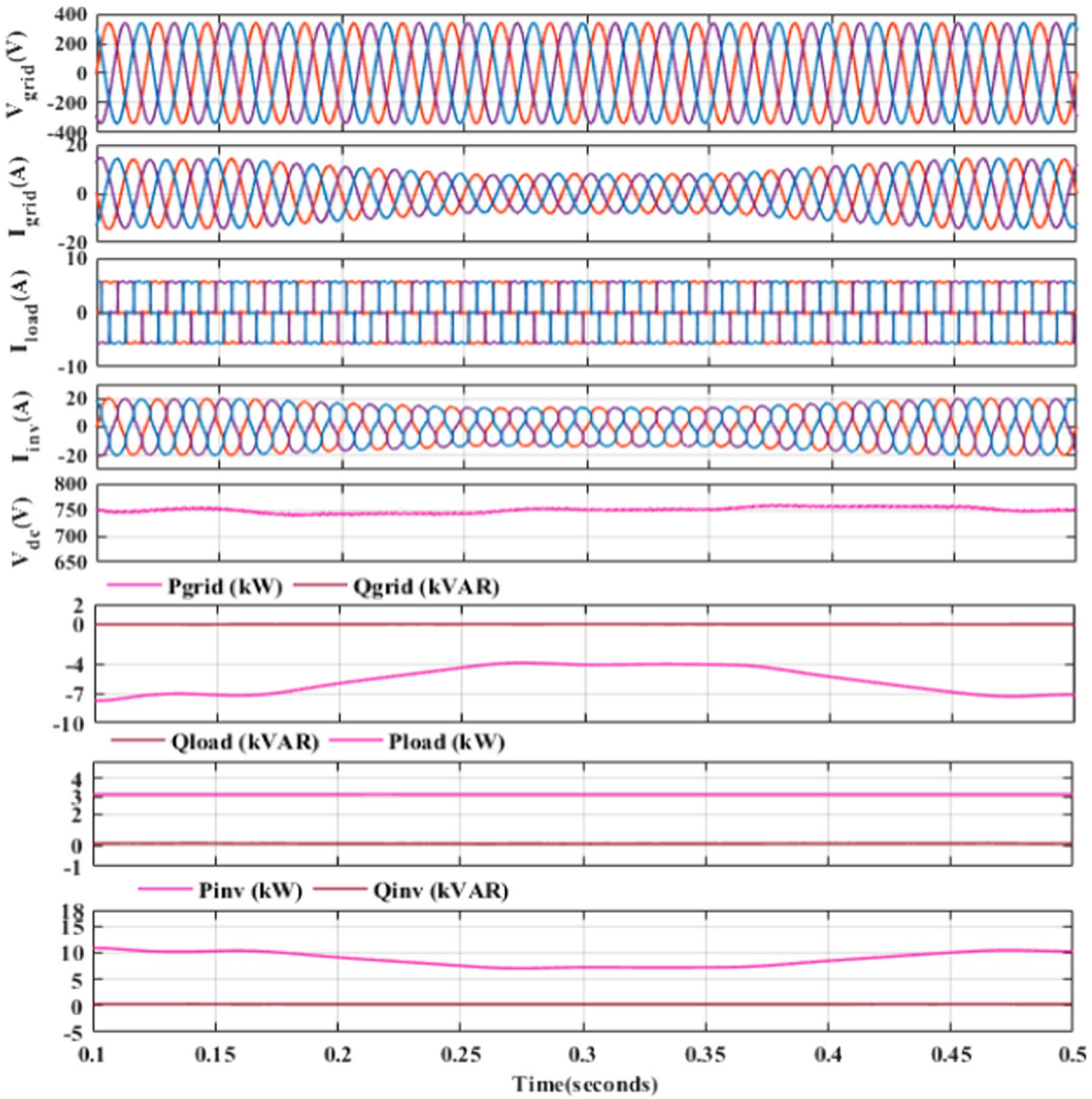

Fig. 10 Simulated performance of SPV-based microgrid under nonlinear load at varying insolation

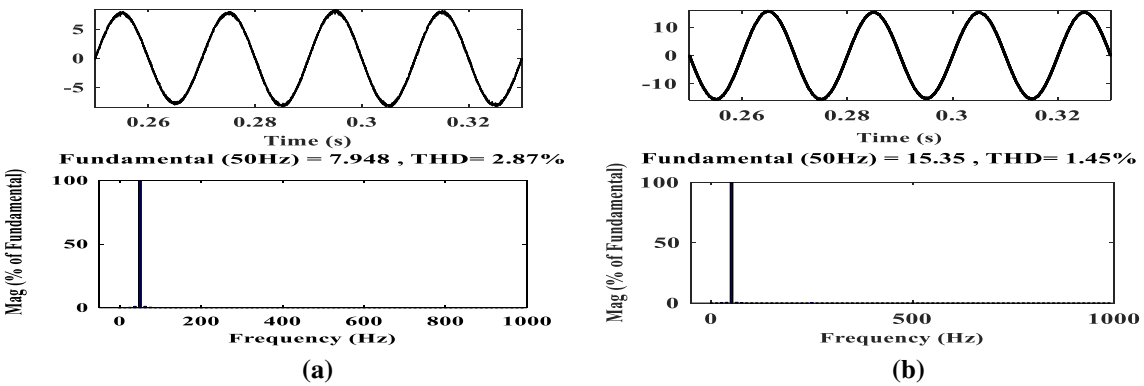

Fig. 11 Grid current waveform and THD at varying insolation: **a** with compensation under linear load, **b** with compensation under nonlinear load

3.1.3 Dynamic Behavior Under Linear and Nonlinear Load-Varying Condition at STC

To test the performance of the proposed controller under variable loads, a linear load of 20 kVA, 0.8 pf lagging (16 kW and 12 kVAR) is connected to the system. It is observed from Fig. 12, V_{grid}, I_{grid} are in phase, showing UPF operation using proposed, IT-2 FLC-based control. V_{dc} is maintained at 750 V. SPV supplies its rated active power of 10.25 kWb and remaining 5.75 kW active power demand of load is supplied by grid, whereas total reactive power is supplied by inverter alone which reduces reactive power drawn from the grid to zero, and hence, IT-2 FLC-based control is efficient in maintaining pf of grid at unity. Further, to test the robustness of the controller under varying load conditions, extra load of 5 kVA, 0.8 pf is connected at 0.2 s. It has been observed that active and reactive load demand is shared between inverter and grid. Power sharing between grid, inverter and load are given in Table 4 and Fig. 12. Under load-varying condition THD (%) in grid current is 1.45%, which is well within IEEE standard 519-2014. Hence, the proposed control is efficient in reducing grid current harmonics and reactive power compensation.

To test the robustness of the proposed control for nonlinear loads, a nonlinear load of a three-phase bridge rectifier with RL load ($R = 100\ \Omega$, $L = 100$ mH) is connected. A linear load of 5kVA, 0.8pf lag is added at 0.15 s and then removed at 0.35 s as shown in Fig. 13. The proposed controller is also able to withstand the load-varying condition, and UPF operation is maintained. Along with this, grid current is sinusoidal in every event of operation. Power sharing between grid, inverter and load are given in Table 5.

3.1.4 Dynamic Behavior Under Linear/Nonlinear (Unbalanced) Load Condition at STC

The performance of grid-integrated SPV system at standard test condition (STC) using proposed IT-2 FLC under linear/nonlinear (unbalanced) load condition is studied, and various parameters of the system, viz., V_{grid}, I_{grid}, I_{load}, I_{inv}, P_{grid}, Q_{grid}, P_{inv}, Q_{inv}, P_{load}, Q_{load}, and V_{dc} are analyzed and presented in Figs. 14 and 15, respectively. Inverter acts as a load balancer by minimizing the unbalanced in grid current while sharing the power between load and grid during single phasing in three-phase system. Figures 14 and 15 show the performance of proposed IT-2 FLC for linear unbalanced and nonlinear unbalanced load, respectively. For analysis of IT-2 FLC controller on unbalanced or single phasing condition, one phase is kept open between 0.15 and 0.35 s. It has been observed during single phasing, inverter supplies, load current as per each phase requirement and keep grid current balanced. Also, it supplies reactive power demand of load and hence keeps grid at UPF. THD in grid current is also maintained at 2.40% and 1.71%, respectively, in both the cases as shown in Fig. 16 which is well within IEEE standard 519-2014.

4 Discussion

It is observed from the analysis and discussion of solar PV integration to grid, voltage across DC link capacitor is regulated using PI controller, type-1 FLC. THD in grid current is improved significantly as compared to that of the conventional PI controller, in case of FLC-based control of DC link voltage. But, with incorporation of IT-2 FLC, improvements in THD value in grid current and voltage are much better in comparison with that of FLC and PI controller. Figure 17a, b shows THD (%) of grid voltage and grid current, respectively, for PI controller, type-1 FLC and IT-2 FLC algorithms. THDs were observed under five different conditions, i.e., linear, nonlinear, varying load, linear unbalanced and nonlinear unbalanced. Performance of the IT-2 FLC controller justifies its superiority relative to PI and type-1 FLC controller in terms of THD in grid current and voltage both.

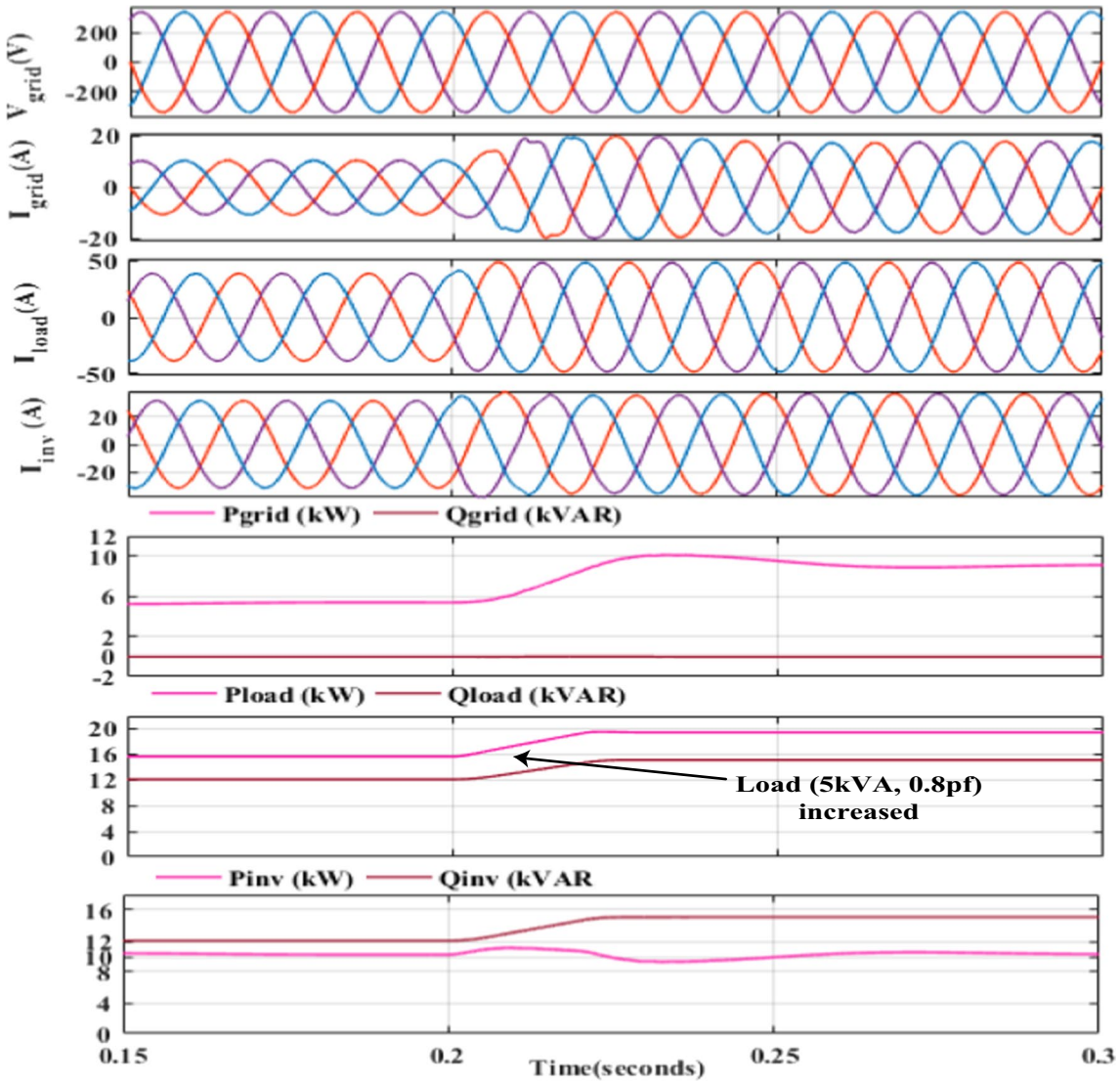

Fig. 12 Simulated performance of SPV-based microgrid under varying linear load at STC input

Table 4 Power sharing between grid, inverter and load for varying load at STC

Till 0.2 s						After 0.2 s					
Grid		Inverter		Load		Grid		Inverter		Load	
P_{grid}	5.75 kW	P_{inv}	10.25 kW	P_{load}	16 kW	P_{grid}	9.75 kW	P_{inv}	10.25 kW	P_{load}	20 kW
Q_{grid}	0 kVAR	Q_{inv}	12 kVAR	Q_{load}	12 kVAR	Q_{grid}	0 kVAR	Q_{inv}	15 kVAR	Q_{load}	15 kVAR
V_{pcc}	340 (peak)	V_{pcc}	340 (peak)	V_{pcc}	340 V (peak)	V_{pcc}	340 V(peak)	V_{pcc}	340 V(peak)	V_{pcc}	340 (peak)
I_{grid}	10A (peak)	I_{inv}	30A (peak)	I_{load}	40A (peak)	I_{grid}	20A (peak)	I_{inv}	30A (peak)	I_{load}	50A (peak)

Transient response of DC link voltage using IT-2 FLC-based control is compared with type-1 FLC and PI controller as shown in Fig. 18. System load has been increased from 20 kVA, 0.8 pf to 25 kVA, 0.8 pf lag at 0.2 s. It is observed from Table 6 that settling time of transient is similar for all three algorithms during grid integration and load variation, respectively. Further, during grid integration, type-1 FLC and PI controller suffer from large overshoot and under shoot, whereas IT-2 FLC has smaller overshoot and undershoot both. Also, PI controller reflects more oscillations as observed in Fig. 18. Hence, IT-2 FLC-based control has best transient responses during grid integration of solar PV

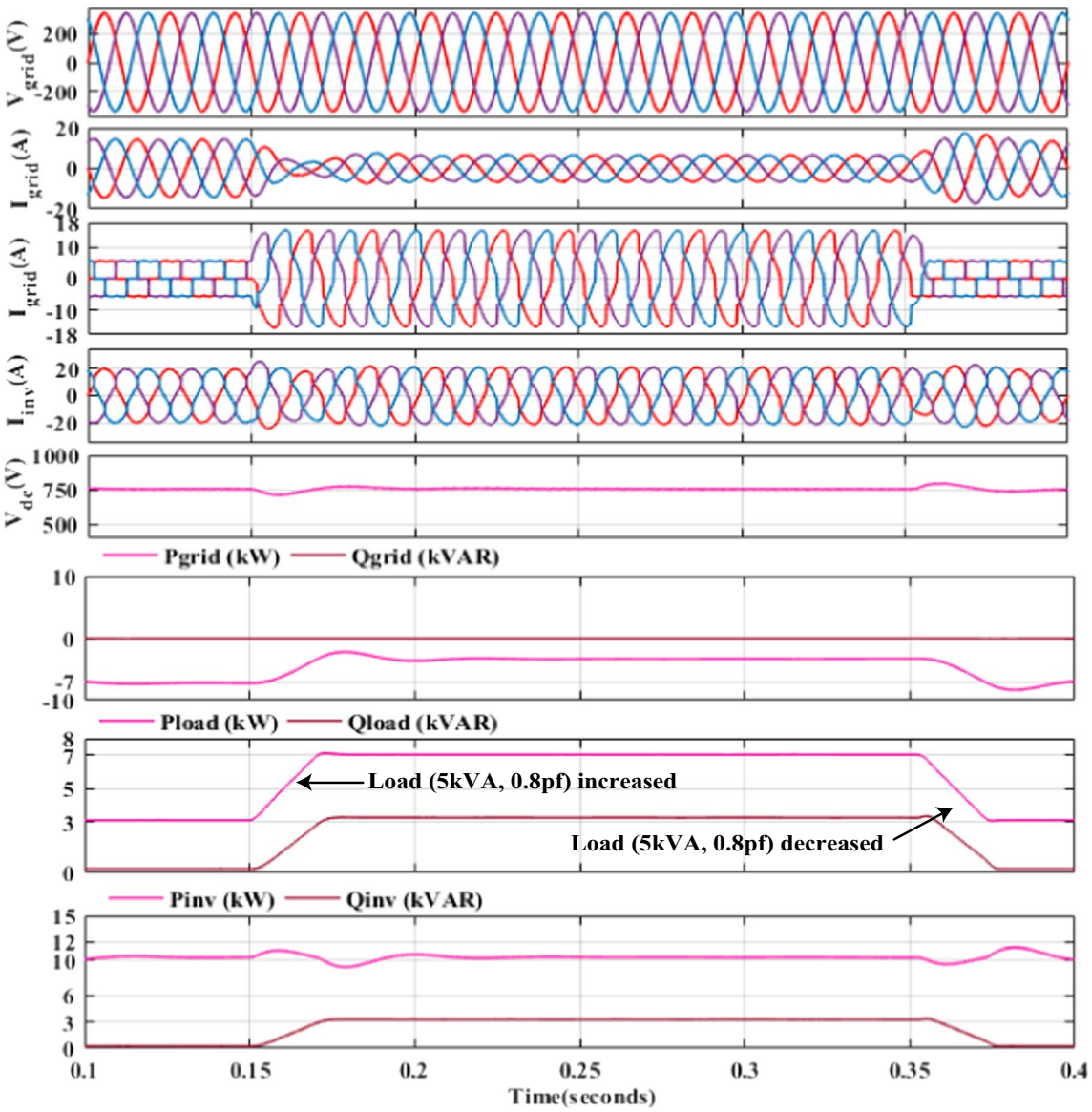

Fig. 13 Simulated performance of SPV-based microgrid under varying nonlinear load at STC input

Table 5 Power sharing between grid, inverter and load for varying load at STC

Till 0.15 s						After 0.15 s					
Grid		Inverter		Load		Grid		Inverter		Load	
P_{grid}	− 7.25 kW	P_{inv}	10.25 kW	P_{load}	3 kW	P_{grid}	− 3.25 kW	P_{inv}	10.25 kW	P_{load}	7 kW
Q_{grid}	0 kVAR	Q_{inv}	0 kVAR	Q_{load}	0 kVAR	Q_{grid}	0 kVAR	Q_{inv}	3 kVAR	Q_{load}	3 kVAR
V_{pcc}	340 V (peak)	V_{pcc}	340 V (peak)	V_{pcc}	340 V (peak)	V_{pcc}	340 V(peak)	V_{pcc}	340 V(peak)	V_{pcc}	340 V (peak)
I_{grid}	− 14A (peak)	I_{inv}	20A (peak)	I_{load}	6A (peak)	I_{grid}	− 7A (peak)	I_{inv}	23A (peak)	I_{load}	16A (peak)

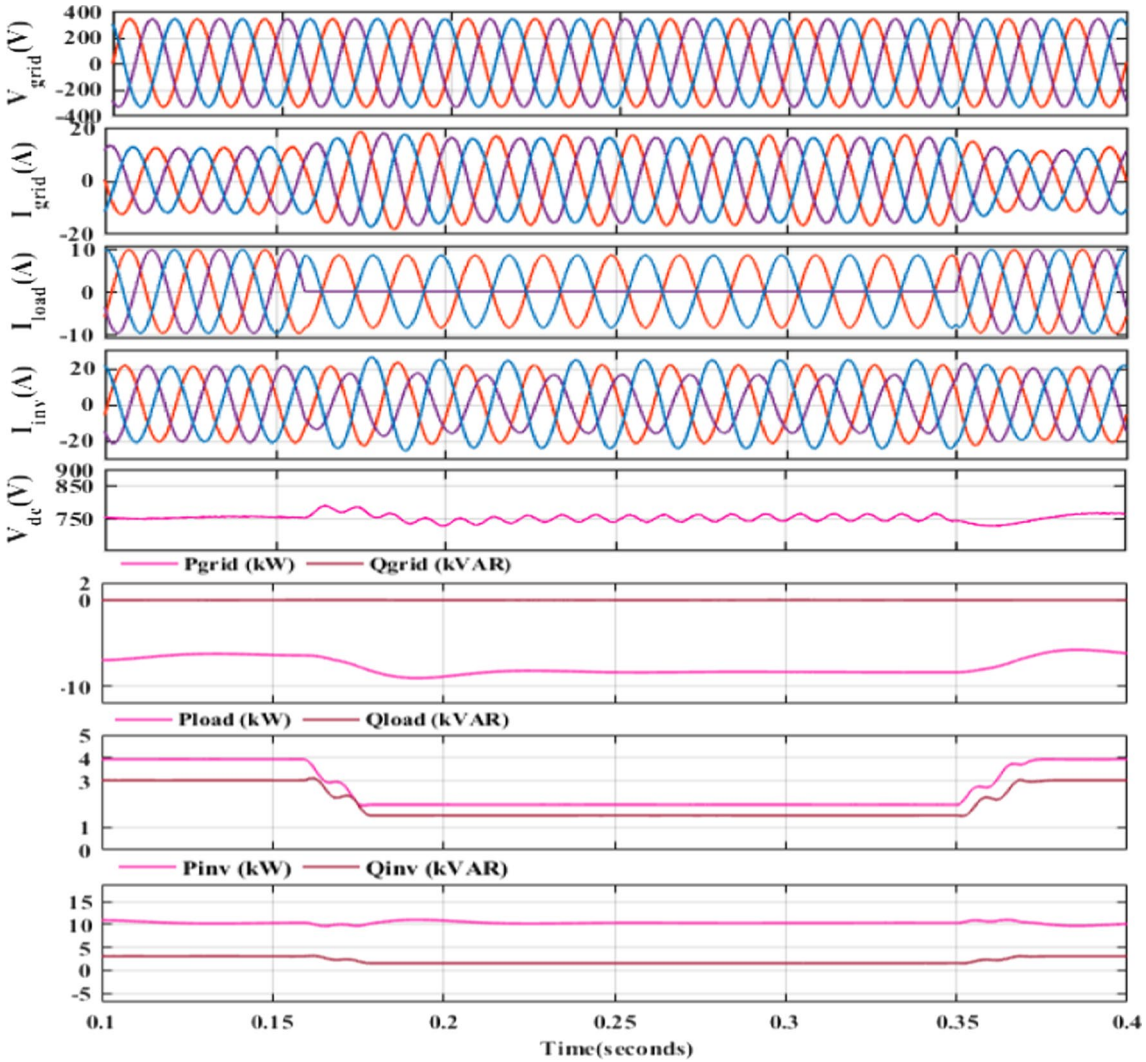

Fig. 14 Simulated performance of SPV-based microgrid under linear unbalanced load at STC input

system. It is observed from Table 7 that during the load variation, transient response of IT-2 as compared to that of type-1 FLC has slightly better response in terms of undershoot and overshoot both while overshoot of PI control is slightly poor and undershoot is slightly better than other, but PI control has more oscillations. Settling time of all three algorithms during load variation is same. Hence, IT-2 FLC-based control has best transient responses during load variation also.

5 Conclusion

In this paper, a novel modified SRF control of SPV-based microgrid using IT-2 FLC algorithm is proposed. The performance of the proposed algorithm is tested on linear/nonlinear/balanced/unbalanced load at both STC and varying insolation condition. Further, the IT-2 FLC has been proposed to compensate the harmonics and reactive power demand of the load. Simulation investigations justify effectiveness of the controller. It has been observed that under all conditions, UPF operation is maintained as well THD are well within the IEEE standards. The proposed IT-2 FLC has significantly improved the power quality of the system under nonlinear load to 1.44% while load current THD is 28.29%, whereas, in case of type-1 FLC and conventional PI control, THD was found to be 1.71% and 1.76%, respectively. With IT-2 FLC, transient response in DC link voltage during load variation has been improved and it is found to be 706 V (undershoot) − 765 V, (overshoot), whereas in case of type-1 FLC and conventional PI control it was found to be 703 V–767 V and 714 V–770 V, respectively. In the future study, IT-2 FLC can be designed for further improvement in PQ and reactive power compensation. Also, high

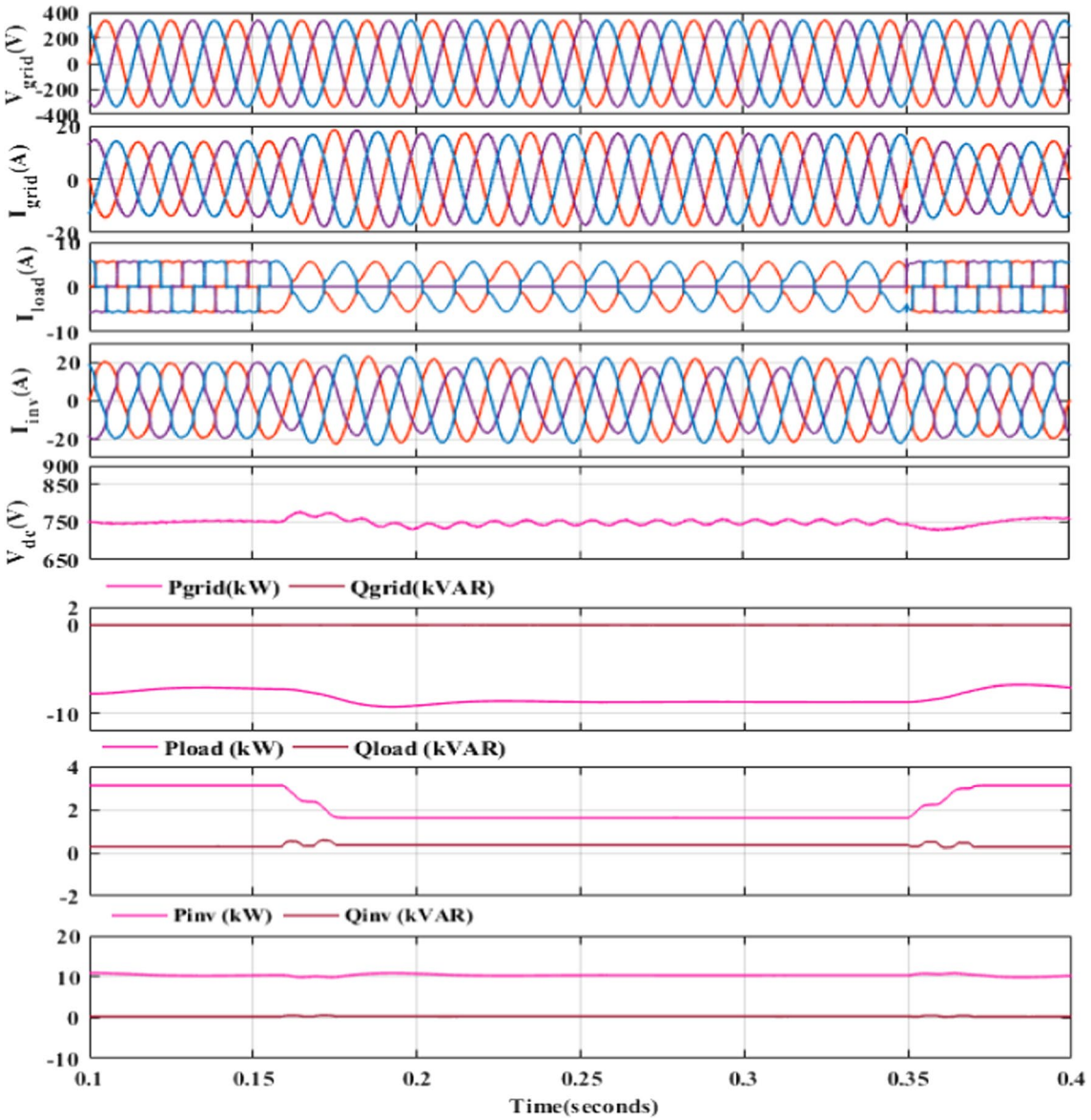

Fig. 15 Simulated performance of SPV-based microgrid under nonlinear unbalanced load at STC input

speed controllers like OPAL-RT OP5142 may be used for the implementation of interval type-2 FLC in real time. This technique shall be helpful in design and implementation of SPV-based microgrid.

Appendix A

Parameters of the system Grid voltages (V_{sabc}): 415 V, frequency (f): 50 Hz, Line impedances (R_s, L_s): 0.01 Ω, 0.1 mH, interfacing inductor (Lf): 7 mH, DC link capacitor (C_{dc}): 500 µF, DC link voltage (V_{dc}): 750 V; solar PV parameters: maximum power of PV array (P_{mp}):10.25 kW, array voltage at MPP (V_{mpp}):410 V, array current at MPP (I_{mpp}): 25 A, DC–DC (boost) converter parameters: duty cycle (D): 0.43, switching frequency (f_s): 10 kHz, inductor (L): 0.5 mH, capacitor (C): 1000 µF,

Different loads: linear load (balanced/unbalanced): 5 kVA, 0.8 pf lag (unbalanced imposed between 0.15 to .35 s),Nonlinear load (balanced/unbalanced): Three-phase bridge rectifier $R = 100$ Ω, $L = 100$ mH (unbalanced imposed between 0.15 to 0.35 s), varying load: (a) 20 kVA, 0.8 pf lag + 5 kVA, 0.8 pf lag (imposed between 0.2 to 0.35 s.), (b) Nonlinear load +5 kVA, 0.8 pf lag (imposed between 0.15 to 0.35 s.)

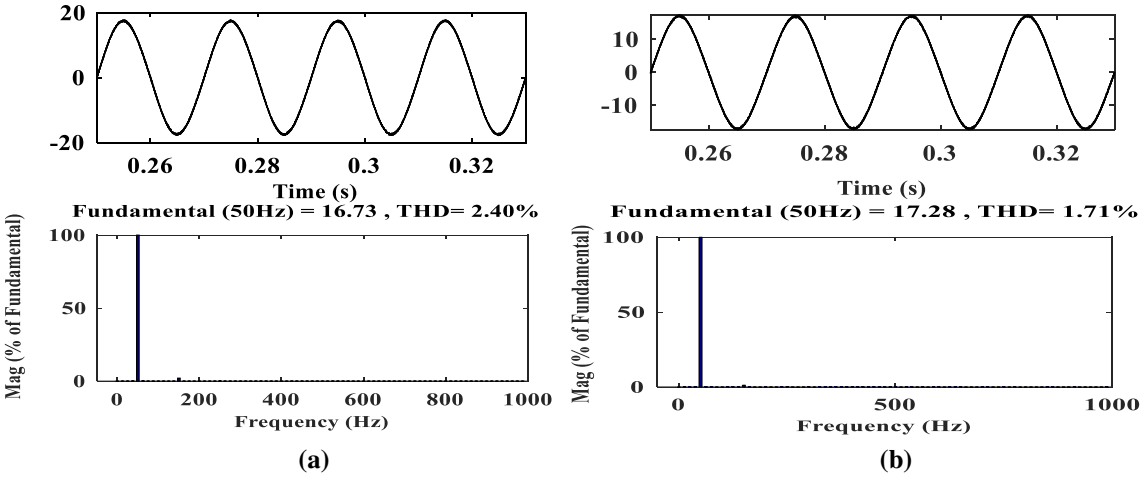

Fig. 16 Grid current waveform and THD at STC input: **a** with compensation under linear unbalanced and **b** with compensation under nonlinear unbalanced load

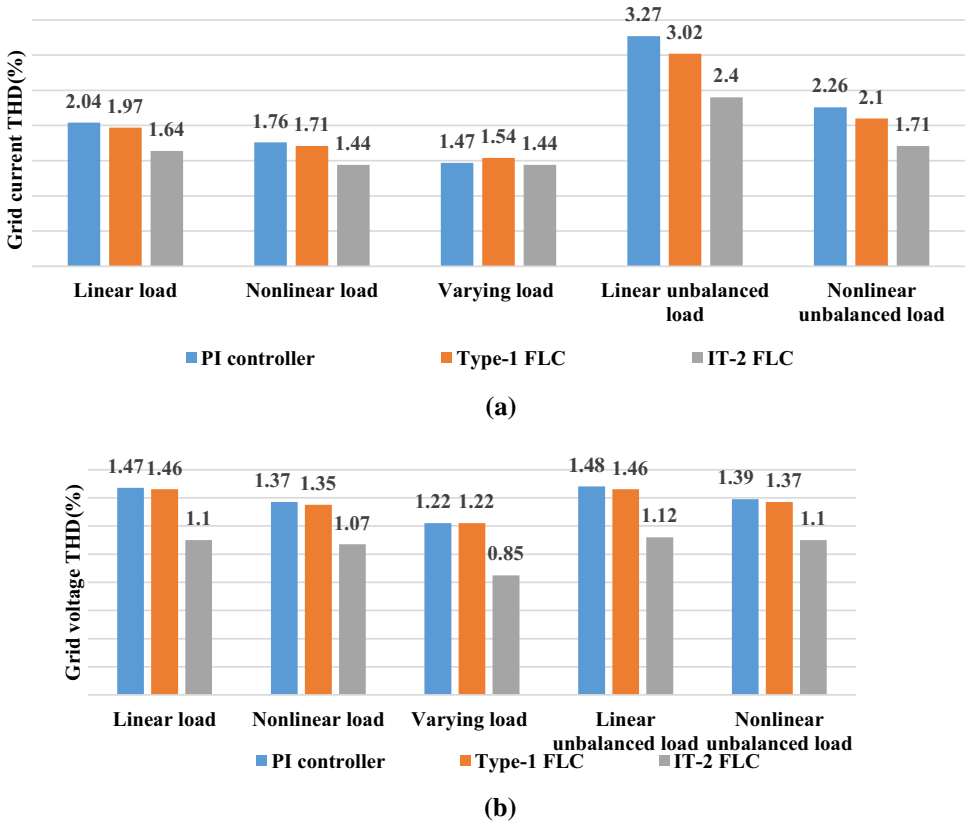

Fig. 17 Comparison of THD in grid current and voltage of various controllers at STC input **a** THD in grid current **b** THD in grid voltage

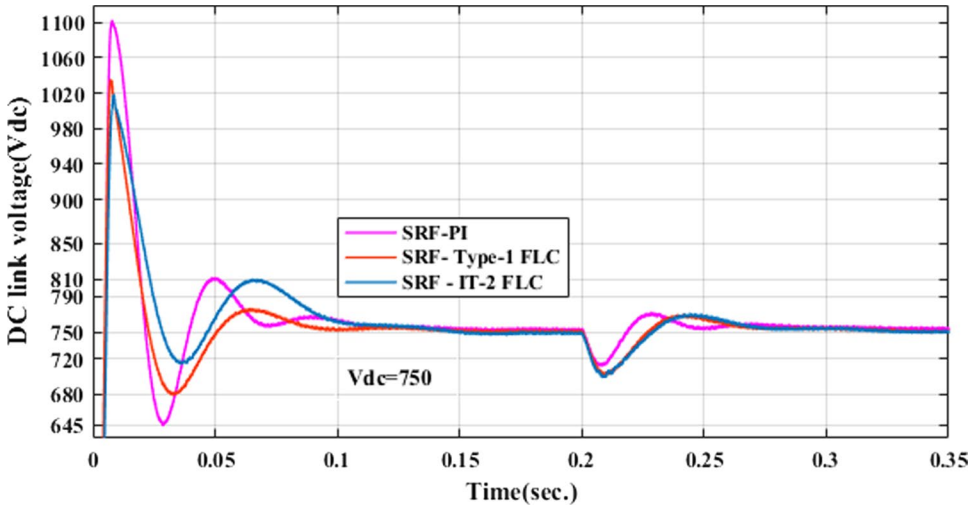

Fig. 18 Transient response of the DC link voltage of different algorithms

Table 6 Transient response during initial SPV grid integration

Controller	Settling time(s)	DC link voltage undershoot(V)	DC link voltage overshoot(V)
SRF PI controller	0.11	645	1100
SRF type-1 FLC	0.11	680	1035
SRF IT-2 FLC	0.11	720	1019

Table 7 Transient response during load variation

Controller	Settling time (s)	DC link voltage undershoot (V)	DC link voltage overshoot (V)
SRF PI controller	0.06	714	770
SRF type-1 FLC	0.06	703	767
SRF IT-2 FLC	0.06	706	765

References

1. Strache, S.; Wunderlich, R.; Heinen, S.: A comprehensive, quantitative comparison of inverter architectures for various PV Systems, PV cells, and irradiance profiles. IEEE Trans. Sustain Energy **5**, 813–822 (2014). https://doi.org/10.1109/TSTE.2014.2304740
2. Lupangu, C.; Bansal, R.C.: A review of technical issues on the development of solar photovoltaic systems. Renew. Sustain. Energy Rev. **73**, 950–965 (2017). https://doi.org/10.1016/j.rser.2017.02.003
3. Shukl, P.; Singh, B.: Grid integration of three-phase single-stage PV system using adaptive laguerre filter based control algorithm under non-ideal distribution system. IEEE Trans. Ind. Appl. **55**(6), 1–9 (2019). https://doi.org/10.1109/tia.2019.2931504
4. Verma, P.; Garg, R.; Mahajan, P.: Asymmetrical fuzzy logic control based mppt algorithm for stand-alone photovoltaic system under partially shaded conditions. Int. J. Sci. Technol. (2019). https://doi.org/10.24200/sci.2019.51737.2338
5. Singh, Mukhtiar; Khadkikar, Vinod; Chandra, Ambrish; Varma, Rajiv K.: Grid interconnection of renewable energy sources at the distribution level with power-quality improvement features. Trans. Power Deliv. **26**(1), 307–315 (2011)
6. Al-Shetwi, A.Q.; Sujod, M.Z.: Grid-connected photovoltaic power plants: a review of the recent integration requirements in modern grid codes. Int. J. Energy Res. **42**(5), 1849–1865 (2018). https://doi.org/10.1002/er.3983
7. Beniwal, N.; Hussain, I.; Singh, B.: Second-order volterra-filter-based control of a solar PV-DSTATCOM system to achieve lyapunov's stability. IEEE Trans. Ind. Appl. **55**(1), 670–679 (2019)
8. Karimi, M.; Mokhlis, H.; Naidu, K.; Uddin, S.; Bakar, A.H.A.: Photovoltaic penetration issues and impacts in distribution network: a review. Renew. Sustain. Energy Rev. **53**, 594–605 (2016). https://doi.org/10.1016/j.rser.2015.08.042
9. Liang, X.: Emerging power quality challenges due to integration of renewable energy sources. IEEE Trans. Ind. Appl. **53**(2), 855–866 (2017)
10. Kumar, P.: Simulation of custom power electronic device D-STATCOM -a case study. In: India Int Conf Power Electron IICPE 2010, pp. 1–4 (2011)
11. Liang, X.; Andalib-Bin-Karim, C.: Harmonics and mitigation techniques through advanced control in grid-connected renewable energy sources: a review. IEEE Trans. Ind. Appl. **54**(4), 3100–3111 (2018)
12. IEEE: IEEE Recommended Practices and Requirements for Harmonic Control in Electrical Power Systems, vol. 1992, pp. 519–1992. IEEE Std, Piscataway (1993)
13. Choi, W.; Lee, W.; Han, D.; Sarlioglu, B.: New configuration of multifunctional grid-connected inverter to improve both current-based and voltage-based power quality. IEEE Trans. Ind. Appl. **54**(6), 6374–6382 (2018)
14. IEEE Std 1547:2003. IEEE Standard for Interconnecting Distributed Resources With Electric Power Systems. IEEE Std 1547-2003.2014, pp. 1–16 (2003)
15. Ounnas, D.; Ramdani, M.; Chenikher, S.; Bouktir, T.: An efficient maximum power point tracking controller for photovoltaic systems using takagi-sugeno fuzzy models. Arab. J. Sci. Eng. **42**(12), 4971–4982 (2017)
16. Trishan, E.; Patrick, L.C.: Comparison of photovoltaic array maximum power point tracking techniques. IEEE Trans. Energy Convers. **22**(2), 439–449 (2007). https://doi.org/10.1109/TEC.2006.874230

17. Jiang, Y.; Abu Qahouq, J.A.; Haskew, T.A.: Adaptive step size with adaptive-perturbation-frequency digital MPPT controller for a single-sensor photovoltaic solar system. IEEE Trans. Power Electron **28**(7), 3195–3205 (2013)
18. Motahhir, S.; EL Hammoumi, A.; EL Ghzizal, A.; Derouich, A.: A open hardware/software test bench for solar tracker with virtual instrumentation. Sustain Energy Technol. Assess. **31**(February), 9–16 (2019). https://doi.org/10.1016/j.seta.2018.11.003
19. El Hammoumi, A.; Motahhir, S.; El Ghzizal, A.; Chalh, A.; Derouich, A.: A simple and low-cost active dual-axis solar tracker. Energy Sci. Eng. **6**(5), 607–620 (2018)
20. Verma, P.; Garg, R.; Mahajan, P.: Asymmetrical interval type-2 fuzzy logic control based MPPT tuning for PV system under partial shading condition. ISA Trans. (2020). https://doi.org/10.1016/j.isatra.2020.01.009
21. Yada, H. K.; Murthy, M. S. R.: An improved control algorithm for DSTATCOM based on single-phase SOGI-PLL under varying load conditions and adverse grid conditions. In: IEEE Int Conf Power Electron Drives Energy Syst PEDES 2016, pp. 1–6 (2017)
22. Singh, B.; Jayaprakash, P.; Kothari, D.P.; Chandra, A.; Al Haddad, K.: Comprehensive study of dstatcom configurations. IEEE Trans. Ind. Inf. **10**(2), 854–870 (2014)
23. Singh, B.; Chandra, A.; Al-haddad, K.: Power Quality Problems and Mitigation Techniques. Wiley (2015). http://onlinelibrary.wiley.com/book/10.1002/9781118922064, ISBN: 978-1-118-92205-7
24. Singh, B.; Shahani, D. T.; Verma, A. K.: Power balance theory based control of grid interfaced solar photovoltaic power generating system with improved power quality. In: PEDES 2012 - IEEE Int Conf Power Electron Drives Energy Syst (2012)
25. Barik, P.K.; Shankar, G.; Sahoo, P.K.: Power quality assessment of microgrid using fuzzy controller aided modified SRF based designed SAPF. Int. Trans. Electr. Energy Syst. **30**(4), 1–24 (2019). https://doi.org/10.1002/2050-7038.12289
26. Karuppanan, P.; Mahapatra, K.K.: PI and fuzzy logic controllers for shunt active power filter a report. ISA Trans. **51**(1), 163–169 (2012). https://doi.org/10.1016/j.isatra.2011.09.004
27. Gupta, N.; Garg, R.; Kumar, P.: Asymmetrical fuzzy logic control to PV module connected micro-grid. In: 12th IEEE Int Conf Electron Energy, Environ Commun Comput Control (E3-C3), INDICON 2015, vol 4, pp. 1–6 (2016)
28. Lee, C.C.: Fuzzy logic in control systems: fuzzy logic controller, part II. IEEE Trans. Syst. Man Cybern. **20**(2), 419–435 (1990)
29. Gupta, N.; Garg, R.: Tuning of asymmetrical fuzzy logic control algorithm for SPV system connected to grid. Int. J. Hydrog. Energy **42**(26), 16375–16385 (2017). https://doi.org/10.1016/j.ijhydene.2017.05.103
30. Pullaguram, D.; Bhattacharya, S.; Mishra, S.; Senroy, N.A.: Fuzzy assisted enhanced control for utility connected rooftop PV. IFAC-Papers OnLine. **50**(1), 7693–7698 (2017). https://doi.org/10.1016/j.ifacol.2017.08.1144
31. Zhu, Y.; Fei, J.: Adaptive Global Fast Terminal Sliding Mode Control of Grid-connected Photovoltaic System Using Fuzzy Neural Network Approach. IEEE Access, vol. 5(c), pp. 9476–84 (2017)
32. Mohamed, A.A.S.; Metwally, H.; El-Sayed, A.; Selem, S.I.: Predictive neural network based adaptive controller for grid-connected PV systems supplying pulse-load. Sol. Energy **193**(September), 139–147 (2019). https://doi.org/10.1016/j.solener.2019.09.018
33. Farhat, M.; Hussein, M.; Atallah, AM.: Enhancement performance of a three phase grid connected photovoltaic system based on pi-genetic algorithm (pi-ga) controller. In: 2017 19th Int Middle-East Power Syst Conf. MEPCON 2017 - Proc.;2018-February(December), pp. 145–51 (2018)
34. Li, X.; Wen, H.; Hu, Y.; Jiang, L.: A novel beta parameter based fuzzy-logic controller for photovoltaic MPPT application. Renew Energy. **130**, 416–427 (2019)
35. Suryanarayana, H.; Mishra, M.K.: Fuzzy logic based supervision of DC link PI control in a DSTATCOM. In: 2008 Annual IEEE India Conference, pp. 1–6 (2008). https://doi.org/10.1109/INDCON.2008.4768766